Research Square

Preprints are preliminary reports that have not undergone peer review.
They should not be considered conclusive, used to inform clinical practice,
or referenced by the media as validated information.

Exploring the mechanism of action of catalpol on the rat model of diabetic erectile dysfunction via transcriptome sequencing

Kangming Cen
The First Clinical College of Guizhou University of Traditional Chinese Medicine
Mengxian Tian
The First Clinical College of Guizhou University of Traditional Chinese Medicine
Jiancheng Zhai
The First Clinical College of Guizhou University of Traditional Chinese Medicine
Pingyu Ge
The First Clinical College of Guizhou University of Traditional Chinese Medicine
Bangwei Che
The First Clinical College of Guizhou University of Traditional Chinese Medicine
Jun Shen
The First Clinical College of Guizhou University of Traditional Chinese Medicine
Jinjun He
The First Clinical College of Guizhou University of Traditional Chinese Medicine
Kaifa Tang
doc.tangkf@hotmail.com

The First Clinical College of Guizhou University of Traditional Chinese Medicine

Article

Keywords: Diabetes Mellitus Erectile Dysfunction, Catalpol, Key genes, Molecular docking

Posted Date: April 19th, 2026

DOI: https://doi.org/10.21203/rs.3.rs-8230997/v1

License: This work is licensed under a Creative Commons Attribution 4.0 International License. Read Full License

Additional Declarations: No competing interests reported.

Abstract

Erectile dysfunction (ED) is common in diabetes mellitus (DM) patients. Catalpol can improve diabetic conditions, but its regulatory mechanisms for DM-induced ED (DMED) are unknown. This study analyzed transcriptomic data to identify catalpol-related genes and mechanisms, aiming to support new therapeutic targets. Differential expression analysis was performed between the Control and DMED groups, and between the DMED and catalpol groups. Common differentially expressed genes 3 (DEGs3) were obtained via Venn diagram analysis. Key genes (KGs) were identified via Protein-Protein Interaction (PPI) network analysis. Their regulatory mechanisms on DMED were explored through chromosomal localization, expression profiling, WebGestalt enrichment, miRNA-KGs network construction, and molecular docking simulations. Finally, a rat model was established (divided into control, DMED, and catalpol groups), and the expressions of key genes were verified by Immunohistochemistry (IHC) and Reverse transcription quantitative polymerase chain reaction (RT-qPCR) analyses. Altogether, 786 DEGs1 and 3,084 DEGs2 were detected between Control as opposed to DMED and DMED as opposed to catalpol group, respectively. A total of 378 DEGs3 were identified. Among them,found that Kdr, Vcam1, Sox18, and Emcn were jointly identified as KGs. Chromosomal localization indicated that Vcam1 and Emcn were located on chromosome 2, Sox18 on 3, and Kdr on 14.Compared with the controls, the KGs were upregulated in DMED, but relative to the DMED group, they were downregulated in the catalpol group. Functional enrichment analysis indicated that Vcam1 was involved in pathways such as cell adhesion molecules. The miRNAs-KGs regulatory network showed that 20 miRNAs could regulate Kdr,5 could regulate Vcam1,2 could regulate Sox18,and 9 could regulate Emcn.Molecular docking revealed robust binding energies of -7.3, -5.9, -6.4, and −5.1 kcal/mol for Kdr, Vcam1, Sox18, and Emcn with catalpol, respectively. Finally, the expression levels of both genes and proteins for Kdr, Vcam1, and Emcn were markedly higher in the DMED group than in the control group ($P < 0.05$). These results indicate that catalpol could have therapeutic potential for DMED by regulating the expression of these key factors. Kdr, Vcam1, Sox18, and Emcn offered crucial clues for DMED pathogenesis and targeted therapy.

1. Introduction

Diabetes-induced erectile dysfunction (DMED) has consistently threatened the sexual health of millions of men across different regions, leading to reduced quality of life, anxiety, relationship strain, and financial burden[1]. DMED significantly affects men's lifestyles and creates powerful physical and psychological distress that erodes men's self-confidence, self-esteem, and mental health[2]. Experts predict that a staggering 322 million men worldwide could be affected in the near future [3,4]. Notably, approximately two-thirds of patients with diabetes are significantly affected by it, which highlights the substantial disease burden imposed by DMED and makes it an urgent global health issue [5].The pathogenesis of DMED

is complex. Long-term hyperglycemia can induce vascular injury (endothelial dysfunction), oxidative stress and neuropathy, thereby disrupting the normal physiological process of erection[6]. Chronic energy metabolism disorders can promote the excessive generation of ROS, triggering oxidative stress. This not only reduces the bioavailability of nitric oxide (NO) and hinders vasodilation[7], but also aggravates vascular dysfunction by activating inflammatory responses, promoting lipid peroxidation and endothelial cell apoptosis[8]. Endothelial dysfunction can inhibit smooth muscle relaxation and lead to the replacement of smooth muscle by fibroblasts, which constitutes the direct cause of DMED[9,10]. The core pathological feature lies in the reduction of NO synthesis caused by the dysfunction of vascular endothelial cells [11]. In addition, diabetes can also cause peripheral nerve and autonomic nerve damage—both of which can lead to ED[12, 13].

The first-line treatment for ED in patients with DM is phosphodiesterase type 5 inhibitors (PDE5i).[14]. However, the therapeutic response rate to phosphodiesterase type 5 inhibitors (PDE5i) in erectile dysfunction (ED) is approximately 60–70%, indicating that a substantial proportion of patients (30–35%) are non-responders [15]. Diabetic erectile dysfunction (DMED) represents a primary etiology among these PDE5i-resistant cases [16]. Given the rising prevalence of DMED, developing novel therapeutic approaches is imperative. Consequently, this research seeks to identify alternative treatment strategies for DMED, which may contribute significantly to the early diagnosis, prevention, and mechanistic understanding of this condition.

As a new drug for the prevention and treatment of diabetes, catalpol is a small molecule iridoid compound, which is the main active ingredient of traditional Chinese medicine Rehmannia and has a good prevention and control effect on obesity, hyperlipidemia, and atherosclerosis[17, 18]. It has been found that catalpol has good antioxidant[19], anti-inflammatory[20], anti-apoptotic[21], lowering blood glucose[22,23], blood lipids[24], and protecting the cardiovascular and cerebrovascular system[25,26], and the iridoid skeleton, hydroxyl group, and glycoside group of catalpol are the chemical basis for its antioxidant and anti-inflammatory functions. Xu et al. stablished a rat model of type 2 diabetes mellitus (T2DM) using a high-fat diet and intraperitoneal injection of stroptozotocin (STZ), and found that catalpol can effectively reduce TC, TG, and LDL-C concentrations, while increasing HDLC and adiponectin levels, which can reduce insulin resistance[27,28]. The insulin secretion index of the rats in the catalpol treatment group was increased, and the structure of islet cells was relatively intact, indicating that catalpol could protect pancreatic islet cells and promote insulin secretion. It was found that catalpol can improve glucose metabolism disorders in T2DM rats, reduce fasting plasma glucose (FPG), and maintain glucose metabolism homeostasis, and catalpol also has the effect of improving insulin sensitivity in T2DM rats[29]. A study using a STZ-induced high-fat and high-glucose rat model found that intravenous injection of catalol (50 mg/kg) could significantly improve the oxidative stress

state of the model. Catalol effectively restored the balance of the oxidative and antioxidant systems by reversing the decline in antioxidant enzyme levels induced by STZ, thereby improving the oxidative damage caused by glycolipid metabolism disorders[30]. However, the mechanism of action of catalpol on DMED is unknown, and this study aims to explore the specific biological functions and molecular mechanisms of catalpol on DMED.

This study commenced with the division of rats into three cohorts: a control group, a DMED model group, and a catalpol intervention group. Following the establishment of the DMED model, systemic blood glucose levels and pathological alterations in penile tissue were evaluated. Subsequently, transcriptomic sequencing of penile tissues from the three groups was conducted to identify differentially expressed genes associated with catalpol's intervention. The biological functions and interactions of the pivotal genes were elucidated through analyses of key signaling pathways, protein-protein interaction (PPI) networks, and miRNA-mRNA regulatory networks. Furthermore, molecular docking simulations were employed to assess the binding affinity between catalpol and the key gene-encoded proteins. Finally, the expression levels of these key genes were validated using reverse transcription quantitative polymerase chain reaction (RT-qPCR) and immunohistochemistry (IHC). The identification of these genes offers potential novel targets for the early diagnosis of DMED, and this study provides valuable insights for further exploration of catalpol's mechanism of action and the clinical management of DMED.

2. Results

2.1High-quality of transcriptome data

The quality of the raw transcriptome sequencing data was rigorously evaluated (**Table S3.Transcriptional Data Evaluation**). The Q20 and Q30 scores of all samples exceeded 97%, and the GC content was consistently maintained within the optimal range of 40–60%, meeting the requirements for downstream analysis (**Table S4.GC Content Evaluation**). In addition, the ridge plot revealed that the expression density distributions among samples were consistent, with most transcripts concentrated within the defined FPKM range, indicating a conserved expression hierarchy (Fig. 1A). The box plot and violin plot further confirmed the comparability of the overall expression distributions among samples (Fig. 1B-C). Collectively, these quality metrics validated the robustness of the transcriptome sequencing data, laying the foundation for subsequent bioinformatics exploration.

2.2 Identification of DEGs upon catalpol intervention

Differential expression analysis between DMED and control samples identified 786 DEGs1, comprising 395 upregulated and 391 downregulated genes in the DMED samples. (Fig. 2A-B, **Table S5.Differential expression analysis between DMED group and control group samples**). In the catalpol intervention group, 3,084 DEGs2 were gained compared with the DMED group, among which 1351 genes were upregulated and 1,733 genes were downregulated

(Fig. 2C-D, **Table S6.Differential expression analysis between DMED group and catalpol group samples)**.Subsequently, a total of 271 overlapping genes were obtained by taking the intersection of 395 upregulated genes in DEGs1 and 1,733 downregulated genes in DEGs2 (Fig. 2E). All in all, 116 overlapping genes were derived by taking the intersection of 391 downregulated genes in DEGs1 and 1,351 upregulated genes in DEGs2 (Fig. 2F). These two sets of overlapping genes were combined, and a total of 387 DEGs3 related to catalpol intervention were finally obtained.

2.3 Functional pathways of the DEGs1, DEGs2, and DEGs3 related to catalpol intervention

DEGs1 were enriched in a total of 1,068 GO biological functions, including 929 in GO-BP, such as chromosome segregation and nuclear chromosome segregation, 58 in GO-CC, such as kinetochore, chromosome, and 81 in GO-MF, such as microtubule binding, tubulin binding (P adjust < 0.05) **(Fig. 3A_1-A_2,Table S7.Biological functions of DEGs1).** In terms of KEGG pathways, the top 15 significantly enriched pathways for DEGs1 included Cell cycle, Motor proteins, Leukocyte transendothelial migration, etc (P adjust < 0.05)(**Fig. 3B_1-B_2,Table S8.The top 15 significantly enriched pathways for DEGs1)**.

DEGs2 were enriched in a total of 2,038 GO biological functions, including 1,732 in GO-BP, such as extracellular structure & matrix organization, 110 in GO-CC, such as extracellular matrix and collagen matrixand, 196 in GO-MF, such as cell adhesion binding and integrin binding (P adjust < 0.05) (**Fig. 3C_1-C_2,Table S9.Biological functions of DEGs2**). In terms of KEGG pathways, the top 15 remarkably aggregated pathways for DEGs2 included cell adhesion molecules, muscle cytoskeleton and cytokine-receptor interaction, etc (P adjust $<$ 0.05) (**Fig. 3D_1-D_2,Table S10.The top 15 significantly enriched pathways for DEGs2**).

A total of 823 GO biological functions were enriched from DEGs3, with 718 in GO-BP, such as endothelium development and ossification, 36 in GO-CC, such as external encapsulating structure, and 69 in GO-MF, such as DNA-binding transcription activator activity (P adjust $<$ 0.05) (**Table S11.Biological functions of DEGs3**). Based on P adjust < 0.05, 17 KEGG pathways were enriched in candidate genes (**Table S12.The top 17 significantly enriched pathways for DEGs3)**. For KEGG, DEGs3 were substantially concentrated in Cell adhesion molecules and Rap1 signaling pathway (Fig. 3E).

2.4 Central analysisand Chromosome Mapping Analysis

A total of 242 CGs1 were screened out from the PPI network (Fig. 4A). The network diagram constructed based on the MCODE analysis consisted of 242 nodes and 516 edges. Among them, a closer connection was found among 15 genes such as Kdr, Angpt1, and Eng (Fig. 4B). The CytoNCA analysis revealed that the three centrality indices, namely Degree, Eigenvector, and Betweenness, all conformed to the power-law distribution, suggesting that

there were a few hub nodes with high centrality in the network (**Fig. 4C$_1$-C$_3$**). The number of genes in the top 5% of Degree, Eigenvector, and Betweenness was 12 CGs3, 12 CGs4, and 12 CGs5, respectively. Furthermore, the results showed that the correlation coefficient between Degree and Eigenvector was 0.770, that between Degree and Betweenness was 0.848, and that between Betweenness and Eigenvector was 0.734, which confirmed that the highly connected nodes played a crucial role in the network, and there was a strong correlation among their characteristics (**Fig. 4D$_1$-D$_3$**).By integrating 4 screening methods (MCODE, Degree, Eigenvector, and Betweenness), it was found that Kdr, Vcam1, Sox18, and Emcn were jointly identified as KGs (Fig. 4E). Chromosomal localization indicated that Vcam1 and Emcn were located on chromosome 2, Sox18 on 3, and Kdr on 14 (Fig. 4F).

2.5KGs expression analysis

The results of the Wilcoxon rank-sum test analysis indicated that the expression levels of the KGs in the samples of DMED exhibited a remarkably elevation compared to those in the control group. Conversely, the expression levels of KGs in the catalpol intervention samples were substantially lower when compared with those in the DMED samples ($P < 0.05$). Catalpol intervention led to no remarkable divergence in KGs expression between the Control and treated groups. (Fig. 5A)

2.6 WebGestalt Enrichment analysis

The gene ontology analysis revealed that only Vcam1 was enriched in 19 related pathways, including 10 in the BP category, 5 in the CC category, and 4 in the MF category. These pathways encompassed leukocyte tethering or rolling and others ($P < 0.05$) (Fig. 5B). Pathway analysis indicated that 4 genes were enriched in 5 related pathways, such as the Cell adhesion molecules pathway and others ($P < 0.05$) (Fig. 5C), clarifying the crucial roles of the KGs in life activities.

2.7 GeneMANIA Analysis

GeneMANIA (http://www.genemania.org/) predicted a total of 20 proteins that had interaction relationships with the proteins encoded by the KGs, namely Osgep, Lgals3, II13, Ezr, Map6, Cyyr1, Adgrl4, Tie1, Ptprb, Kcnj8, Mmrn2, Sox17, Adgrf5, Sox7, Egfl7, Plxnd1, Cyb5a, Rasgrp3, Mapk3, and Tmem204. Among them, Lgals3, II13, and Ezr all had the function of early endosome to late endosome transport with Vcam1. A significant predicted relationship was found between Osgep and both Sox18 and Emcn. Strong physical interactions were detected between Plxnd1, Map6, Mapk3 and Kdr. Co-expression relationships were present among most of these proteins(Fig. 5D).These results revealed the potential biological functions of the KGs and the possibly existing functionally associated genes, providing important clues for the analysis of the action mechanisms of the KGs.

2.8 miRNA-KGs regulatory network

The prediction results from the miRWalk and Targetscan databases indicated that 20 key miRNAs, including rno-miR-195-5p, were predicted for Kdr. Five key miRNAs, such as rno-miR-455-3p, were forecasted for Vcam1. Two key miRNAs, like rno-miR-652-5p, were projected for Sox18. And nine key miRNAs, including rno-miR-103-3p, were anticipated for Emcn (Fig. 5E**- F**). These results facilitated the revelation of the regulatory effects of miRNAs on KGs during biological processes such as disease occurrence and progression.

2.9 molecular docking

The strongest binding energies of the molecular docking simulations between Kdr, Vcam1, Sox18, Emcn and the catalpol molecule were − 7.3, -5.9, -6.4, and − 5.1 kcal/mol, respectively (**Table 1.Molecular docking of catalpal with core genes Kdr, Vcam1, Sox18, Emcn**).In the molecular docking simulation between the KGs and catalpol, it was found that there were two amino acid residues between Kdr and catalpol, namely leucine (LEU) at position 836 and cysteine (CYS) at position 915 (Fig. 6A). Between Vcam1 and catalpol, three amino acid residues were identified: tyrosine (TYR) at 143, arginine (ARG) at 147, and isoleucine (ILE) at 201 (Fig. 6B). With respect to Sox18 and catalpol, four amino acid residues were detected: aspartic acid (ASP) at 75, glutamic acid (GLU) at 76, arginine (ARG) at 80, and leucine (LEU) at 135 (Fig. 6C). Regarding Emcn and catalpol, four amino acid residues were observed: aspartic acid (ASP) at 75, glutamic acid (GLU) at 76, arginine (ARG) at 80, and leucine (LEU) at 135 (Fig. 6D). These results helped to reveal the relationship between the compounds and specific KGs.

2.10Assessment of rat model

After the rat model was established, the weight data revealed that the weight of the control group increased gradually, while the weight of the DMED group and Catalpol group increased slowly following STZ injection. The blood glucose data showed that the blood glucose levels of the Control group remained relatively stable, whereas the blood glucose levels of the DMED and Catalpol groups increased significantly after STZ-induced modeling (Fig. 7A-C). Subsequently, ELISA test results indicated that the DMED group had significantly higher concentrations of SHBG and TNF-α compared to the Control group ($P < 0.0001$), suggesting an increased inflammatory response. In contrast, the SOD concentration was significantly lower in the DMED group, indicating elevated oxidative stress **(**Fig. 7D-F**)**. However, in the catalpol intervention group, the concentrations of SHBG and TNF-α were significantly reduced compared to the DMED group, while the SOD concentration was significantly higher. These findings suggested that Catalpol might have a therapeutic effect on DMED.

Histological analysis via HE staining further supported these observations. The Control group exhibited normal penile corpora cavernosa without obvious septa. In contrast, the DMED group showed significant septa formation in the penile corpora cavernosa, with disordered and loose arrangements of blood sinuses, endothelial cells, and smooth muscle cells. The number of smooth muscle cells decreased, collagen fibers increased markedly, and

interstitial tissue proliferated extensively and irregularly. In the Catalpol group, the penile corpora cavernosa tissue showed signs of improvement and repair, with a higher number of red blood cells in the penile corpora cavernosa vessels compared to the DMED group. However, the improvement in connective tissue was not as pronounced (Fig. 7G).

2.11 The gene and protein levels expression of key genes

RT-qPCR analysis revealed that the gene expression levels of Kdr, Vcam1, and Emcn were significantly higher in the DMED group compared to the control group ($P < 0.01$) (Fig. 8A-C). This upregulation suggested that DMED was associated with increased expression of these genes, which might contribute to the underlying pathological processes. However, in the catalpol intervention group, the expression levels of Kdr, Vcam1, and Emcn were significantly decreased compared to the DMED group ($P < 0.05$ for all three genes) (Fig. 8A-C). This finding indicated that catalpol might exert therapeutic effects by downregulating these genes, potentially mitigating the adverse effects of DMED.

IHC further supported these observations, showing pronounced protein expression of Kdr, Vcam1, and Emcn in the DMED group ($P < 0.05$) (Fig. 8D-I). The elevated protein levels of these genes in DMED tissues (compare to control group) were consistent with their increased gene expression and highlighted their potential role in the pathogenesis of DMED. The reduced expression in the catalpol intervention group (compare to DMEP group) further supported the notion that catalpol can modulate these key factors, thereby improving the pathological conditions associated with DMED.

3. Discussion

Catalpol, a iridoid glucoside, is the main active ingredient derived from Rehmannia root. Catalpol has a variety of pharmacological effects, including analgesic, sedative, hepatoprotective, laxative, anti-inflammatory, antimicrobial, antitumor, and anti-apoptosis[34]. Studies have shown that diabetic rats showed a significant reduction in blood glucose levels after intravenous injection of catalpol, specifically, catalpol modulates gluconeogenesis through the PI3K/AKT pathway and inhibits glucosamine-induced gluconeogenesis by down-regulating enzymes involved in gluconeogenesis, thereby improving glucose uptake and glucose metabolism in the liver of diabetic patients[35]. Erectile dysfunction is a complication of diabetes, and patients with diabetes develop erectile dysfunction earlier and have more severe symptoms[36]. However, the specific mechanism of action of catalpol in DMED is unknown. This study explores the gene regulatory mechanism of Ziyuan in treating DMED based on transcriptome data from the control group, DMED group, and Ziyuan intervention group. Using bioinformatics, it analyzes the expression levels, biological functions, protein networks with similar effects, and molecular docking binding

activity with Ziyuan for key genes (Kdr, Vcam1, Sox18, and Emcn), providing new reference for the diagnosis and treatment of DMED.

The results of this study show that the DMED group had significantly increased concentrations of Sex Hormone-Binding Globulin (SHBG) and Tumor Necrosis Factor-alpha (TNF-α), indicating an increased inflammatory response. In contrast, the DMED group had significantly decreased SOD concentrations, indicating elevated oxidative stress. However, in the Catalpol intervention group, compared to the DMED group, the concentrations of SHBG and TNF-α were significantly reduced, while SOD concentrations were significantly increased. These findings suggest that Catalpol may have therapeutic effects on DMED. Sex hormone-binding globulin (SHBG) is a glycoprotein that can transport androgens such as testosterone. Its levels in the body are mainly regulated by two mechanisms: insulin inhibits its synthesis and secretion, while cortisol plays a stimulating role[37]. In diabetic patients, hyperinsulinemia caused by insulin resistance inhibits the liver's synthesis of SHBG, significantly reducing the SHBG content in the body. This not only disrupts the circulation and metabolism of sex hormones but also aggravates the disorder of glycolipid metabolism and insulin resistance, forming a vicious cycle [38,39]. Oxidative stress plays a key role in the pathogenesis of ED. SOD is a key antioxidant enzyme for scavenging superoxide anion radicals and is regarded as an important marker of oxidation reactions[40,41]. Multiple studies have consistently found in different ED models (such as aging, diabetes, and cavernous nerve injury) that the activity of SOD in penile tissue or serum is significantly reduced, while the content of MDA is significantly increased [42,43]. These evidences of evidence indicate that oxidative stress imbalance plays a significant role in the pathogenesis of various ED rat models, and correcting oxidative stress imbalance is an important way to improve ED. TNF-α is an important endogenous pro-inflammatory factor. Its concentration in the plasma of ED patients increases and is positively correlated with the severity of ED. The pathogenic mechanism lies in that TNF-α can promote lipid peroxidation and superoxide anion generation by up-regulating the expression and activity of NADPH oxidase, thereby leading to a decrease in the expression of nitric oxide synthase (nNOS and eNOS) and a reduction in eNOS activity in the corpus cavernosum, ultimately damaging the smooth muscle relaxation mechanism and weakening penile erectile function[44]. Animal experiments have confirmed that the spongy smooth muscle relaxation ability of TNF-α gene knockout mice is enhanced, while injecting TNF-α into normal mice weakens their erectile function[45]. Therefore, TNF-α has been confirmed to be involved in the occurrence and development of DMED and may be an important pathogenic factor[46].

Microvascular complications in diabetes arise from diabetic microangiopathy as their underlying pathological mechanism. The Kinase Insert Domain Receptor (Kdr), alternatively designated as vascular endothelial growth factor receptor 2 (VEGFR-2), serves as the primary mediator of VEGF-induced angiogenesis and plays an essential role in endothelial cell differentiation. KDR has tyrosine kinase activity, which can mediate the proliferation,

invasion, and migration of endothelial cells and improve vascular permeability and neovascularization when activated by conjugation to VEGFA, VEGFC, and VEGFD[47]. In the angiogenesis mechanism, β-catenin can indirectly enhance the expression of KDR by up-regulating the transcription factor Sox17, thereby promoting endothelial cell germination and angiogenesis[48]. Research utilizing the IIEF-5 questionnaire and EPC measurements has demonstrated that diabetic patients with erectile dysfunction display markedly lower CD34 + KDR + CD133 + cell counts compared to diabetic individuals without ED. A positive correlation was observed between IIEF-5 ratings and CD34 + KDR + CD133 + cell quantities. Among type 1 diabetic subjects experiencing ED, diminished levels of CD34 + KDR + CD133 + cells were detected, with cell counts showing correlation with IIEF scores. These observations align with our experimental results.[49].

Vascular Cell Adhesion Molecule 1 (Vcam1) acts as a binding molecule on the surface of the activated endothelium,On the one hand, it promotes the aggregation of inflammatory cells by mediating the rolling and transendothelial migration of white blood cells. On the other hand, its expression is upregulated by various inflammatory factors such as IL-1β and TNF-α, thereby amplifying the inflammatory response [50]. The activation of endothelial cells may also play an important role in the development of diabetes. Studies have shown that the serum VCAM1 concentration in patients with type 2 diabetes is significantly elevated and positively correlated with the severity of proteinuria[51]. Studies have shown that VCAM1 may be a biomarker for transitional obesity and diabetic nephropathy[52]. Mechanistically, hyperinsulinemia upregulates VCAM1 expression by activating the MAPK signaling pathway and induces ROS production, participating in diabetic vascular injury and even neurodegeneration[53,54]. A mechanism study leech and centipede granules (LCG, a traditional Chinese medicine couplet) in STZ-induced DMED rats showed that LCG administration significantly improved erectile function in DMED rats by significantly reducing VCAM-1, ICAM-1, and CD62P, increasing NO production, and inhibiting endothelial cell apoptosis and fibrosis[55].

SRY-box transcription factor 18 (SOX18) is essential for angiogenesis during wound healing and tissue repair. Sox18 is a barrier-induced TF in endothelial cells (EC) that can upregulate Wnt-related signaling and downregulate EC proliferation[56]. Diabetes mellitus affects angiogenesis and endothelial function, and EC subsets with high expression of Sox18, Ly6C, and Kdr play an important role in vascular regeneration, and changes in the function of EC subsets associated with the expression of these genes may affect the progression of diabetes-related vascular lesions[57]. Research has demonstrated that SOX18 gene mutations are linked to hypotrichosis-lymphedema-telangiectasia (HLT) syndrome in human subjects. Similarly, these mutations account for significant cardiovascular abnormalities and hair follicle malformations observed in ragged (RA) mouse models[58,59].

Among the many cell adhesion molecules involved, Endomucin (EMCN) is specifically expressed on the luminal side of postcapillary venous endothelial cells as a membrane-bound glycoprotein and participates in physiological and pathological angiogenesis[60]. Studies have shown that overexpression of EMCN in diabetic retinopathy can reduce leukocyte-endothelial adhesion to improve inflammation and stabilize the retinal barrier to inhibit vascular leakage in rats[61]. This study demonstrated that the gene and protein expression levels of Emcn in the DMED group were significantly higher than those in the control group ($P < 0.05$), which is consistent with previous findings on EMCN in diabetic microvascular dysfunction. In addition, EMCN also plays an important role in the repair of diabetes-related tissues. The specific blood vessels of CD31 + EMCN + in the skin are involved in the regeneration process, and the decline in their quantity is the basis for the impaired angiogenesis in the refractory wounds of diabetes. The activation of such blood vessels by targeting the VEGF/BMP2/Noggin signaling pathway has also been proven to promote the coupling of angiogenesis and osteogenesis in diabetic bone metabolic disorders[62,63,64]. These findings suggest that EMCN is a key molecule in maintaining microvascular function and integrity in a diabetic environment. Therefore, EMCN may play an important role in the development of DMED.

Through functional enrichment analysis of key genes, it was found that the Vcam1 gene-related expression pathway was significant, including Biological Process (BP10), 5 Cellular Component (CC5), and 4 Molecular Function (MF4) terms. Further enrichment analysis of core genes identified 5 related significant pathways, including cell adhesion molecules, NF-kappa B signaling pathway, and Leukocyte transendothelial migration. For example, neurite growth inhibitor-B (Nogo-B) is a modulator that promotes movement and adhesion of vascular endothelial cells in the form of a reticulo-4 subtype by binding to the receptor Nogo-B receptor (NgBR), Indicates that Nogo-B is a regulator of vascular remodeling and angiogenesis[65]. ICAM-1 functions as a glycoprotein adhesion receptor on cell surfaces, mediating leukocyte migration from circulation to inflammatory regions. Beyond its presence on vascular endothelial cells, ICAM-1 can be substantially upregulated in epithelial and immune cells following inflammatory signals[66]. Research has indicated that elevated NgBR and ICAM-1 levels in cavernous tissue of diabetic erectile dysfunction (DMED) rat models are associated with compromised erectile function under hyperglycemic conditions[67]. NF-κB signaling operates through canonical and non-canonical pathways. The alternative pathway, activated by CD40, lymphotoxin β receptors, or BAFF receptors, participates in lymphoid organ development, B lymphocyte maturation, and osteoclast formation. This pathway relies on IKKα phosphorylation, which triggers ubiquitination and proteolytic processing of p100. Mineralocorticoid receptor (MR) blockers may alleviate cavernous tissue injury resulting from aldosterone-MR-NF-κB axis activation[68]. Leukocyte transendothelial migration (TEM) predominantly proceeds via paracellular routes between endothelial cell (EC) junctions. Loss of EC autophagy results in excessive neutrophil TEM and dysregulated leukocyte trafficking in murine inflammation models, whereas autophagy enhancement suppresses neutrophil

tissue infiltration. At the molecular level, autophagy modulates EC junction reorganization and adhesion molecule expression by facilitating their intracellular trafficking and proteolytic breakdown[69].

4. Methods

4.1 Construction of rat model and sample collection

Twenty-one male Sprague-Dawley rats (6–8 weeks, 200–220 g) were obtained from Beijing Huafukang Biotechnology Co., Ltd. (Production License: SCXK (Beijing) 2019-0010; Use License: SYXK (Dian) 2020-0006) .After adapting to feeding for one week under standard conditions at the Experimental Animal Center of Guizhou University of Traditional Chinese Medicine.Randomly allocated into three groups ($n = 5$ each): Control, DMED, and catalpol intervention. DMED and catalpol groups received a high-fat diet for 4 weeks, followed by a single intraperitoneal STZ injection (60 mg/kg). Diabetes induction was confirmed by fasting blood glucose ≥ 16.7 mmol/L at 48 and 72 hours post-injection across three consecutive measurements. Control animals received standard chow for 4 weeks and citrate buffer injection (50 mM, pH 4.5). Post-modeling, the catalpol group received daily catalpol gavage (100 mg/kg) for 8 weeks, Catalpol was purchased from RENI Pharmaceutical Technology Co., Ltd (batch number: TC1081-231018).while Control and DMED groups received equivalent volumes of saline. Animals were monitored weekly for adverse effects throughout the intervention. After the intervention, prepare Shutai 50 into a working solution of 50 mg/mL, weigh the rats, and calculate the required volume of the medication. According to the recommended initial dose of 40 mg/kg (calculated based on Shutai 50 raw material), the working fluid (50 mg/mL) is injected intraperitoneally at 0.8 mL/kg. About 3–5 minutes after injection, the animal gradually enters deep anesthesia. After confirming no pain response, euthanasia is performed using cervical dislocation method. Penile tissue was rapidly collected, with some frozen at -80 ° C and some fixed with 4% paraformaldehyde for subsequent analysis.

All experimental procedures involving rats in this study followed the ethical principles of animal experimentation in the Helsinki Declaration and were approved by the Animal Ethics Committee of Guizhou University of Traditional Chinese Medicine (approval number: 20250829001). During the experiment, a standard anesthesia protocol was used to reduce animal pain, and the animal's condition was closely monitored after surgery. All operations were carried out in accordance with the institution and ARRIVE guidelines[70,71].

4.2 transcriptomic sequencing data analysis

Total RNA extraction was performed using Trizol reagent (Thermo Fisher, 15596018). RNA quantity and integrity were evaluated with the Bioanalyzer 2100 system and RNA 6000 Nano LabChip Kit (Agilent, CA, USA, $5067-1511$). Samples with RNA Integrity Number (RIN) > 7.0 were selected for library preparation. Poly(A) mRNA was enriched from 5 µg total RNA

through two rounds of purification with Dynabeads Oligo (dT) (Thermo Fisher, CA, USA). Ribosomal RNA depletion and RNA fragmentation were achieved using the Magnesium RNA Fragmentation Module (NEB, cat.e6150, USA). First-strand cDNA synthesis was performed using SuperScriptTM II Reverse Transcriptase (Invitrogen, cat.1896649, USA). Following adapter ligation, libraries were PCR-amplified and sequenced on the Illumina NovaseqTM 6000 platform with 150 bp paired-end sequencing.

4.3 Quality control of transcriptomic data

To ensure data reliability and minimize technical and systematic biases, quality control measures were implemented for all sequencing data. Cutadapt (version 1.9) was employed to remove low-quality reads, followed by quality assessment using FastQC (version 0.11.9) [72]. to evaluate Q20, Q30 scores, and GC content of the cleaned data. Expression quantification was performed by calculating FPKM values through StringTie and ballgown (http://www.bioconductor.org/packages/release/bioc/html/ballgown.html), which facilitated transcript and gene expression profiling. Cross-sample normalization was applied to both read counts and transcript lengths. Gene expression distribution patterns were displayed through ridgeline, violin, and box plots using the ggplot2 package (version 3.4.1)[73].

4.4 Identification of Differentially Expressed Genes (DEGs1, DEGs2, DEGs3)

In transcriptome sequencing data, the DEGs1 and DEGs2 were discovered between DMED and control samples, along with between catalpol intervention and DMED samples, using the DESeq2 package (v 1.38.0)[74]with criteria of $|\log_2 FC| > 1$ and $P\,\text{adjust} < 0.05$. Subsequently, the ggplot2 package (v 3.4.1) was employed to generate the volcano plot for the DEGs1 and DEGs2, while the ComplexHeatmap package (v 2.14.0) was utilized to visua[75]lize the heatmap for the DEGs1 and DEGs2. The top 10 most significantly up - and down-regulated genes, ordered by descending $\log_2 FC$ values, were annotated on the volcano plot, and their expression profiles were simultaneously represented in the accompanying heatmap.

The intersections were taken between the up - regulators of DEGs1 and the down - regulators of DEGs2, as well as between the latter's up - regulators and the former's down - regulators. Then, the genes from these two intersections were merged to obtain the DEGs3 The above results were visualized using the package ggvenn (v 0.1.9)[76].

4.5 Functional pathways of the DEGs1, DEGs2, and DEGs3

To elucidate the biological functions of catalpol-responsive DEGs1, DEGs2, and DEGs3, Gene Ontology (GO) enrichment analysis was conducted using clusterProfiler (v 4.10.0)[77] in combination with org.Rn.eg.db (version 3.16.0)[78]. The analysis encompassed three GO categories: biological processes (BP), cellular components (CC), and molecular functions

(MF). Additionally, Kyoto Encyclopedia of Genes and Genomes (KEGG)[79,80,81] pathway enrichment was performed (P adjust < 0.05). For each analysis, the top 5 significantly enriched pathways were presented in ascending order of adjusted P-values.

4.6 Central analysisand Chromosome Mapping Analysis

Protein-protein interaction (PPI) networks for DEGs3 were constructed using the STRING database (https://string-db.org/) with a confidence score threshold of ≥ 0.4. After excluding unmatched and isolated nodes, the retained genes were designated as candidate genes 1 (CGs1). Module detection within CGs1 was performed using MCODE with the following parameters: Degree Cutoff = 2, Node Score Cutoff = 0.2, K-Core = 2, and Max Depth = 100. Genes within significant modules were classified as candidate genes 2 (CGs2). Network centrality analysis of CGs1 was executed using CytoNCA, calculating three topological metrics: Degree, Eigenvector, and Betweenness centrality. Density distributions of these metrics were visualized using ggplot2 (v 3.4.1). The top 5% of genes ranked by Degree, Eigenvector, and Betweenness were designated as CGs3, CGs4, and CGs5, respectively. Correlation analysis among these gene sets was performed using the cor function from the stats package (v 4.2.2) and visualized with ggplot2. The intersection of CGs2, CGs3, CGs4, and CGs5 across the four analytical approaches was displayed as an UpSet plot using UpSetR (v 1.4.0)[82], with genes identified by all four methods defined as key genes (KGs). Finally, chromosomal positions of KGs were mapped using the RCircos package[83].

4.7 KGs expression analysis

The Wilcoxon test function in the package stats (v 4.2.2) was used to perform Wilcoxon rank sum test on the expression of KGs between the Control and DMED samples, between the DMED and catalpol samples, and between the Control and catalpol samples. The threshold was set at a P - value of < 0.05.

4.8 WebGestalt Enrichment analysis

The KGs were subjected to functional distribution and pathway enrichment analysis using the WebGestalt database (https://www.webgestalt.org/). The parameters were sequentially selected as "BP", "CC", and "MF" in GO, and "KEGG" in pathway. Results with a p-value $<$ 0.05 were considered significant. The results related to GO and pathway were visualized using the ggsankey packages (v 0.099999) and ggplot2 (v 3.4.1) for sankey diagram and general visualization respectively.

4.9 GeneMANIA Analysis

To understand the interactions and functions between the proteins encoded by KGs and other related proteins, a concurrent expression network of KGs was constructed via GeneMANIA (http://www.genemania.org/).

4.10 miRNA-KGs regulatory network

Putative miRNA regulators of KGs were identified by integrating predictions from miRWalk (http://mirwalk.umm.uni-heidelberg.de) and TargetScan (https://www.targetscan.org/vert_80/) databases. Overlapping predictions from both platforms were designated as key miRNAs and visualized using UpSetR (V 1.4.0). The mRNA-miRNA regulatory network was constructed using ggsankey.

4.11 molecular docking

To assess KG-catalpol binding affinity, the three-dimensional structure of catalpol was retrieved from PubChem (https://pubchem.ncbi.nlm.nih.gov/), while AlphaFold-predicted KG protein structures were obtained from UniProt (https://www.uniprot.org/). Docking simulations were executed using CB-Dock (https://cadd.labshare.cn/cb-dock/php), with binding energies below − 5 kcal/mol indicating favorable interactions.

4.12 Hematoxylin and Eosin (HE) staining

Tissue architecture was assessed via hematoxylin and eosin staining. Paraffin-embedded penile sections were deparaffinized, rehydrated, and immersed in hematoxylin for 5 minutes to stain nuclei. After differentiation in acid-alcohol solution (10–15 seconds) and water rinsing (15 minutes), sections were counterstained with eosin (5–10 seconds) to visualize cytoplasm. Following alcohol dehydration, xylene clearing, and neutral resin mounting, histopathological features were examined microscopically.

4.13 Elisa detection

SHBG, SOD, and TNF-α concentrations were quantified by ELISA. Standard curves were established using serial dilutions (50 µL per well). Test samples underwent 5-fold dilution (40 µL diluent + 10 µL sample) prior to loading. After 30-minute incubation at 37°C, wells were washed five times with diluted buffer (30-fold concentrated stock diluted in distilled water). Enzyme-conjugated antibody (50 µL) was added to all wells except blanks, followed by 30-minute incubation at 37°C and washing. Chromogenic substrates A and B (50 µL each) were added for 10-minute dark incubation at 37°C. Stop solution (50 µL) terminated the reaction, converting color from blue to yellow. Absorbance was measured at 450 nm within 15 minutes.

4.14 RT-qPCR analysis

KG expression was validated by RT-qPCR in penile tissues across all groups. Total RNA was isolated using TRIzol reagent (Ambion, USA), and concentration was measured with NanoPhotometer N50. Complementary DNA synthesis was performed using SureScript First-Strand cDNA Synthesis Kit on an S1000™ Thermal Cycler (Bio-Rad, USA). Primer sequences are listed in **(Table S1.The primer sequence of RT-qPCR)**. Amplification was conducted on CFX Connect Real-Time PCR System (Bio-Rad, USA) with the following cycling conditions:

initial denaturation at 95°C for 2 minutes, followed by 40 cycles of 95°C for 10 seconds, 60°C for 30 seconds (annealing), and 60°C for 30 seconds (extension). Relative expression was calculated using the 2^(-ΔΔCT) method. Data were analyzed and visualized in GraphPad Prism (V 10.1.2) with significance set at $P < 0.05$.

4.15 IHC staining

KG protein expression was examined by immunohistochemistry. Following decalcification, penile tissues were fixed in 4% paraformaldehyde (24–48 hours), then processed through alcohol dehydration, xylene clearing, paraffin infiltration, and embedding. Sections were deparaffinized at 64°C for 1 hour, cleared in xylene, rehydrated through graded alcohols, and subjected to heat-induced antigen retrieval. Endogenous peroxidase was quenched with 3% hydrogen peroxide. After blocking with 5% BSA at 37°C, sections were incubated with primary antibodies (**Table S2.Primary antibodies of IHC**) diluted in 2% BSA, followed by reaction enhancer (100 µL) and anti-mouse IgG polymer. Chromogenic detection employed DAB substrate with hematoxylin counterstaining (5 minutes). Sections were then dehydrated, cleared, mounted, and digitally scanned for analysis.

4.16 Statistical Analysis

All statistical analyses were performed in R (V 4.2.2). Inter-group comparisons were conducted using Wilcoxon tests with significance threshold of $P < 0.05$.

5. Summary and outlook

In this study, the key gene targets of catalpol intervention in erectile dysfunction were identified via gene sequencing of rats in DMED group, blank control group, and catalpol intervention group. The experimental results showed that the effect of catalpol on erectile dysfunction in diabetic rats was to effectively scavenge free radicals and reduce alleviates oxidative stress through antioxidants. The QPCR results showed that Kdr, Vcam1 and Emcn were up-regulated in the DMED group, indicating that catalpol has a certain therapeutic effect on vascular damage, angiogenesis abnormalities and inflammatory responses caused by diabetes, helping to improve angiogenesis, reduce inflammatory responses and repair vascular endothelium, and repair the microvascular-related pathological changes in penile tissue caused by diabetes. The results of this study provide new insights for the clinical diagnosis and treatment of DMED patients, but there are certain limitations, such as the small sample size selected in this study, the identified biomarkers need to be verified by large-scale clinical trials, the core genes and catalpol drugs need to be further verified through a series of experiments in vivo and in vitro, etc., and the core targets are further analyzed to analyze the mechanism signaling pathway, and the clinical application of bioinformatics analysis results needs more samples of data support. In addition, we will continue to pay attention to the role of these mechanisms, such as catalpol may improve metabolic disorders and endothelial damage through antioxidant and anti-inflammatory

synergistic effects, and catalpol may inhibit inflammatory adhesion and immune dysregulation.

Declarations

Author Contribution

Kaifa Tang: Funding acquisition, Supervision, Validation, Visualization, Writing-review & editing; Kangming Cen: Funding acquisition, Data curation, Formal analysis, Investigation, Methodology, Project administration, Software, Validation, Visualization, Writing-original draft, Writing-review & editing;Mengxian Tian: Funding acquisition, Data curation, Formal analysis, Methodology, Project administration, Software, Validation, Visualization, Writing-original draft, Writing-review & editing; Jiancheng Zhai: Conceptualization, Investigation, Methodology, Writing-review & editing; Bangwei Che and Pingyu Ge: Funding acquisition, Supervision, Validation, Visualization; Jun Shen and Jinjun He: Supervision, Validation, Visualization.

Data Availability

The raw sequencing data and analysis code generated in this study have been deposited in the NCBI database under the accession number [PRJNA1390441], with the access link [https://www.ncbi.nlm.nih.gov/search/all/?term=PRJNA1390441]. All other original data generated in this study can be reasonably requested from the corresponding author, Kaifa Tang (E-mail: doc.tangkf@hotmail.com).

References

1. Kitaw TA, Abate BB, Tilahun BD, Yilak G, Haile RN. Umbrella review protocol: Global burden and risk factors of erectile dysfunction in diabetic population. Health Sci Rep. 2024 May 30;7(6):e2159. doi: 10.1002/hsr2.2159. PMID: 38826618; PMCID: PMC11139671.
2. Avasthi A, Grover S, Bhansali A, Dash RJ, Gupta N, Sharan P, Sharma S. Erectile dysfunction in diabetes mellitus contributes to poor quality of life. Int Rev Psychiatry. 2011;23(1):93-9. doi: 10.3109/09540261.2010.545987. PMID: 21338304.
3. De Berardis G, Pellegrini F, Franciosi M, Belfiglio M, Di Nardo B, Greenfield S, et al. Longitudinal assessment of quality of life in patients with type 2 diabetes and self-reported erectile dysfunction. Diabetes Care. 2005; 28(11):2637–43.
4. 2.Kitaw TA, Abate BB, Tilahun BD, Yilak G, Rede MB, Getie A, Haile RN. The global burden of erectile dysfunction and its associated risk factors in diabetic patients: an umbrella reviews. BMC Public Health. 2024 Oct 14;24(1):2816. doi: 10.1186/s12889-024-20300-7. PMID: 39402470; PMCID: PMC11472474.

5. Kolluru GK, Bir SC, Kevil CG. Endothelial dysfunction and diabetes: effects on angiogenesis, vascular remodeling, and wound healing. Int J Vasc Med. 2012;2012:918267.
6. overview. Int J Innov Stud Med Sci. 2019; 3(1):13–4.
7. Newsholme P, Haber EP, Hirabara SM, et al. Diabetes associated cell stress and dysfunction: role of mitochondrial and non-mitochondrial ROS production and activity. J Physiol. 2007;583(Pt 1):9–24. doi:10.1113/jphysiol.2007.135871.
8. Kma L, Baruah TJ. The interplay of ROS and the PI3K/Akt pathway in autophagy regulation. Biotechnol Appl Biochem. 2022;69(1):248–264. doi:10.1002/bab.2104.
9. Bhatt MP, Lee YJ, Jung SH, et al. C-peptide protects against hyperglycemic memory and vascular endothelial cell apoptosis. J Endocrinol. 2016;231(1):97–108. doi:10.1530/joe-16-0349.
10. Ma JX, Wang B, Li HS, et al. Uncovering the mechanisms of leech and centipede granules in the treatment of diabetes mellitus-induced erectile dysfunction utilising network pharmacology. J Ethnopharmacol. 2021;265:113358. doi:10.1016/j.jep.2020.113358.
11. Maxwell AJ. Mechanisms of dysfunction of the nitric oxide pathway in vascular diseases. Nitric Oxide. 2002;6(2):101–124. doi:10.1006/niox.2001.0394.
12. Fowler CJ, Ali Z, Kirby RS, Pryor JP. The value of testing for unmyelinated fibre, sensory neuropathy in diabetic impotence. Br J Urol. 1988; 61(1):63–7.
13. Herman WH, Pop-Busui R, Braffett BH, Martin CL, Cleary PA, Albers JW, et al. Use of the Michigan Neuropathy Screening Instrument as a measure of distal symmetrical peripheral neuropathy in type 1 diabetes: results from the Diabetes Control and Complications Trial/Epidemiology of Diabetes Interventions and complications. Diabet Med. 2012; 29(7):937–44.
14. Andersson KE. PDE5 inhibitors—pharmacology and clinical applications 20 years after sildenafil discovery. Br J Pharmacol. 2018; 175(13): 2554-2565. doi:10.1111/bph.14205. PubMed PMID: 29667180; PubMed Central PMCID: PMCPMC6003652.
15. Lee M, Sharifi R. Non-invasive management options for erectile dysfunction when a phosphodiesterase type 5 inhibitor fails. Drugs Aging. 2018;35(3):175–187.
16. F PD, M LD, P LD, et al. Do impotent men with diabetes have more severe erectile dysfunction and worse quality of life than the general population of impotent patients? Results from the exploratory comprehensive evaluation of erectile dysfunction (ExCEED) database. Diabetes Care. 2003;26(4):1093–1099. doi:10.2337/diacare.26.4.1093.
17. Tian X，Ru Q，Xiong Q，et al. Catalpol attenuates hepatic steatosis by regulating lipid metabolism via AMP-activated protein kinase activa， tion[J]. Biomed Res Int，2020，2020，6708061，
18. Ren HH，Wang D，Zhang L，et al. Catalpol induces autophagy and attenuates liver steatosis in ob/ob and high-fat diet-induced obese mice[J]. Aging （Albany NY），2019，11，21，，9461-9477，

19. Zhu HF，Wang Y，Liu ZQ，et al. Antidiabetic and antioxidant effects of catalpol extracted from Rehmannia glutinosa （Di Huang） on rat diabetes induced by streptozotocin and high-fat，high-sugar feed[J]. Chin Med，2016，11，25。
20. Bi FJ，Xu YJ，Chen GX，et al. Anti-inflammatory and Anti endoplasmic reticulum stress effects of catalpol Against myocardial ischemia-reperfusion injury in streptozotocin-induced diabetic rats[J]. An Acad Bras Cienc，2020，92，4，e20191148。
21. Chen YP，Chen J，Jiang M，et al. Loganin and catalpol exert coop， erative ameliorating effects on podocyte apoptosis upon diabetic ne， phropathy by targeting AGEs-RAGE signaling[J]. Life Sci，2020，252， 117653。
22. Bao QW，Shen XZ，Qian L，et al. Anti-diabetic activities of catal， pol in db/db mice[J]. Korean J Physiol Pharmacol，2016，20，2， 153-160。
23. Liu JY，Zheng CZ，Hao XP，et al. Catalpol ameliorates diabetic atherosclerosis in diabetic rabbits[J]. Am J Transl Res，2016，8，10， 4278-4288。
24. Tian X，Ru Q，Xiong Q，et al. Catalpol attenuates hepatic steatosis by regulating lipid metabolism via AMP-activated protein kinase activa， tion[J]. Biomed Res Int，2020，2020， 6708061。
25. Yan JH，Zou GL. Effect of Catalpa on cardiac function and cardiac tis， sue of diabetic cardiomyopathy rats[J]. Jilin J Chin Med，2018，38，5， 573-575。
26. Zhu HF，Wan D，Luo Y，et al. Catalpol increases brain angiogen， esis and up-regulates VEGF and EPO in the rat after permanent middle cerebral artery occlusion[J]. Int J Biol Sci，2010，6，5，443-453。
27. Xu YT. Study on the activation of hypothalamic TAS2R108/PLCβ2 path， way by catalpol mediating TRH/TSH/T3 regulation of lipid metabolism in the liver of high-fat diet mice[D]，Chongqing，Southwest University， 2024.
28. Xu CF，Cao Q，Zhang BF. Catalpol improves insulin resistance and lipid metabolism disorder in diabetic mice by inhibiting microRNA 101-3p to up-regulate FOS-related antigen 2[J/OL]，J Physiol Pharma， col，2024[epub ahead of print]，DOI: 10.26402/jpp.2024.3.05.
29. Shen PY. Mechanism of catalpol regulation of AMPK/GLUT4 signaling pathway in skeletal muscle of rats with type 2 diabetes[D]. Harbin，Hei， longjiang University of Chinese Medicine，2023。
30. Chinese Pharmacopoeia Commission. People’s republic of China （PRC） pharmacopoeia-part ，2020 edition[M]. Beijing，China Medi， cal Science Press，2020。
31. Kanehisa, M. and Goto, S.; KEGG: Kyoto Encyclopedia of Genes and Genomes. Nucleic Acids Res. 28, 27-30 (2000).
32. Kanehisa, M; Toward understanding the origin and evolution of cellular organisms. Protein Sci. 28, 1947-1951 (2019).
33. Kanehisa, M., Furumichi, M., Sato, Y., Kawashima, M. and Ishiguro-Watanabe, M.; KEGG for taxonomy-based analysis of pathways and genomes. Nucleic Acids Res. 51, D587-

D592 (2023).
34. Bhattamisra SK, Yap KH, Rao V, Choudhury H. Multiple Biological Effects of an Iridoid Glucoside, Catalpol and Its Underlying Molecular Mechanisms. Biomolecules. 2019 Dec 24;10(1):32. doi: 10.3390/biom10010032. PMID: 31878316; PMCID: PMC7023090.
35. Bhattamisra SK, Koh HM, Lim SY, Choudhury H, Pandey M. Molecular and Biochemical Pathways of Catalpol in Alleviating Diabetes Mellitus and Its Complications. Biomolecules. 2021 Feb 20;11(2):323. doi: 10.3390/biom11020323. PMID: 33672590; PMCID: PMC7924042.
36. Kouidrat Y, Pizzol D, Cosco T, Thompson T, Carnaghi M, Bertoldo A, Solmi M, Stubbs B, Veronese N. High prevalence of erectile dysfunction in diabetes: a systematic review and meta-analysis of 145 studies. Diabet Med. 2017 Sep;34(9):1185-1192. doi: 10.1111/dme.13403. Epub 2017 Jul 18. PMID: 28722225.
37. Hautanen A. Synthesis and regulation of sex hormone-binding globulin in obesity. Int J Obes Relat Metab Disord. 2000;24 Suppl 2:S64-S70.
38. Tong G, Hua X, Zhong Y, et al. Intensive insulin therapy increases sex hormone-binding globulin in newly diagnosed type 2 diabetic patients. Eur J Endocrinol. 2014;170(2):237-245.
39. Hedderson MM, Xu F, Darbinian JA, et al. Prepregnancy SHBG concentrations and risk for subsequently developing gestational diabetes mellitus. Diabetes Care. 2014;37(5):1296-1303.
40. ZHANG S, XU J, SI H, et al. The Role Played by Ferroptosis in Osteoarthritis: Evidence Based on Iron Dyshomeostasis and Lipid Peroxidation[J]. Antioxidants (Basel), 2022,11(9):1668.
41. IQBAL M J, KABEER A, ABBAS Z, et al. Interplay of oxidative stress, cellular communication and signaling pathways in cancer[J]. Cell Commun Signal, 2024,22(1):7.
42. S Jiang, Q Cai, Y Gao, et al. Trigonella foenum-graecum L. and Psoralea corylifolia L.Improve Erectile Dysfunction in Streptozotocin-Induced Diabetic Rats throughSuppression of Oxidative Stress[J]. Evid Based Complement Alternat Med, 2022, 2022:4187359.
43. S Resim, E Koluş, O Barut, et al. Ziziphus jujube ameliorated cavernosal oxidativestress and fibrotic processes in cavernous nerve injury-induced erectile dysfunction in arat model[J]. Andrologia, 2020, 52: e13632.
44. LONG T,LIU G,WANG Y,et al.TNF-a,erectile dysfunction,and NADPH oxidase-mediated ROS generation in corpus cavernosum in high-fat diet/streptozotocin-induced diabetic rats[J].J Sex Med.2012,9(7):1801-1814.
45. CARNEIRO F S,STURGIS L C,GIACHINI F R,et al.TNF-alpha knockout mice have increased corpora cavernosa relaxation[J].JSexMed,2009,6(1):115-125.
46. HAYWARDMD,JONES BK,SAPAROVA,etal.An extensive phenotypic characterization of the hTNFalpha transgenic mice[J].BMC Physiol,2007,7:13.

47. Tsai ML, Lee CH, Huang LC, Chen YH, Liu WN, Lin CY, Hsu KW, Lee AW, Lin CL. CRISPR-mediated knockout of VEGFR2/KDR inhibits cell growth in a squamous thyroid cancer cell line. FEBS Open Bio. 2022 May;12(5):993-1005. doi: 10.1002/2211-5463.13399. Epub 2022 Apr 8. PMID: 35313079; PMCID: PMC9063427.
48. Martowicz A, Trusohamn M, Jensen N, et al.Endothelial beta-Catenin Signaling Supports Postnatal Brain and Retinal Angiogenesis by Promoting Sprouting, Tip Cell Formation,and VEGFR(VascularEndothelial Growth Factor Receptor) 2 Expression[J].Arterioscler Thromb Vasc Biol, 2019, 39(11):2273-88.
49. Maiorino MI, Bellastella G, Petrizzo M, Della Volpe E, Orlando R, Giugliano D, Esposito K. Circulating endothelial progenitor cells in type 1 diabetic patients with erectile dysfunction. Endocrine. 2015 Jun;49(2):415-21. doi: 10.1007/s12020-014-0478-5. Epub 2014 Nov 20. PMID: 25411101.
50. Wang T, Tian J, Jin Y. VCAM1 expression in the myocardium is associated with the risk of heart failure and immune cell infiltration in myocardium. Sci Rep. (2021) 11:19488. doi: 10.1038/s41598-021-98998-3.
51. Hocaoglu-Emre F.S., Saribal D., Yenmis G., Guvenen G. Vascular cell adhesion molecule 1, intercellular adhesion molecule 1, and the cluster of differentiation 146 levels in patients with type 2 diabetes with complications. Endocrinol Metab. 2017;32(1):99–105. doi: 10.3803/EnM.2017.32.1.99.
52. Bohle A, Wehrmann M, Bogenschütz O, Batz C, Müller CA, Müller GA. The pathogenesis of chronic renal failure in diabetic nephropathy. Investigation of 488 cases of diabetic glomerulosclerosis. Pathol Res Pract. (1991) 187:251–9.
53. Fadel MM, Abdel Ghaffar FR, Zwain SK, Ibrahim HM, Badr EA. Serum netrin and VCAM-1 as biomarker for Egyptian patients with type II diabetes mellitus. Biochem Biophys Rep. 2021 Jun 11;27:101045.
54. Huang J, Lin W, Sun Y, Wang Q, He S, Han Z, Lu L, Kang X, Chen Y, Guo H, Cui Z, Sun C, Go K, Wu J, Yao M, Cao M, Xu Y. Quercetin targets VCAM1 to prevent diabetic cerebrovascular endothelial cell injury. Front Aging Neurosci. 2022 Sep 1;14:944195.
55. Ma JX, Wang B, Ding CF, Li HS, Jiang XJ, Wang CY, Yu J, Chen WQ. Couplet medicines of leech and centipede granules improve erectile dysfunction via inactivation of the CaSR/PLC/PKC signaling in streptozotocin-induced diabetic rats. Biosci Rep. 2020 Feb 28;40(2):BSR20193845.
56. Zhang H, Yamaguchi T, Kawabata K. The maturation of iPS cell-derived brain microvascular endothelial cells by inducible-SOX18 expression. Fluids Barriers CNS. 2023 Feb 2;20(1):10.
57. Li Y, Liu Z, Han X, Liang F, Zhang Q, Huang X, Shi X, Huo H, Han M, Liu X, Zhu H, He L, Shen L, Hu X, Wang J, Wang QD, Smart N, Zhou B, He B. Dynamics of Endothelial Cell Generation and Turnover in Arteries During Homeostasis and Diseases. Circulation. 2024 Jan 9;149(2):135-154.

58. Pennisi D., Gardner J., Chambers D., Hosking B., Peters J., Muscat G., Abbott C., Koopman P. Mutations in Sox18 underlie cardiovascular and hair follicle defects in ragged mice. Nat. Genet. 2000;24:434–437.
59. Carter T.C., Phillips J.S. Ragged, a semidominant coat texture mutant. J. Hered. 1954;45:151–154.
60. Endothelial glycocalyx plays a significant role in the development and progression of diabetic complications. Endomucin (EMCN) is an anti-inflammatory membrane glycoprotein that is mainly expressed in venous and capillary endothelial cells.
61. Niu T, Zhao M, Jiang Y, Xing X, Shi X, Cheng L, Jin H, Liu K. Endomucin restores depleted endothelial glycocalyx in the retinas of streptozotocin-induced diabetic rats. FASEB J. 2019 Dec;33(12):13346-13357.
62. Liu L, Zheng CX, Zhao N, Zhu T, Hu CB, Zhang N, Chen J, Zhang KC, Zhang S, Liu JX, Zhang K, Jing H, Sui BD, Jin Y, Jin F. Mesenchymal Stem Cell Aggregation-Released Extracellular Vesicles Induce CD31+ EMCN+ Vessels in Skin Regeneration and Improve Diabetic Wound Healing. Adv Healthc Mater. 2023 Aug;12(20):e2300019.
63. Wu Z, Hou Q, Qin L, Chen T, Yang K, Wei F, Wang L. GPx-mimetic selenium-enriched yeast nanozymes ameliorate diabetic bone disease via dual-targeting of ROS scavenging and angiogenesis-osteogenesis coupling. Mater Today Bio. 2025 May 6;32:101836.
64. Zeng Q, Liu T, Qin L, Wang C, Peng G, Liu Z, Tao J. Screening of potential hub genes involved in Kidney Wilms tumor via bioinformatics analysis and experimental validation. BMC Cancer. 2024 Jun 27;24(1):771.
65. Zhang Y, Li JJ, Xu R, Wang XP, Zhao XY, Fang Y, Chen YP, Ma S, Di XH, Wu W, She G, Pang ZD, Wang YD, Zhang X, Xie W, Deng XL, Du XJ, Zhang Y. Nogo-B mediates endothelial oxidative stress and inflammation to promote coronary atherosclerosis in pressure-overloaded mouse hearts. Redox Biol. 2023 Dec;68:102944. doi: 10.1016/j.redox.2023.102944. Epub 2023 Oct 21. PMID: 37890359; PMCID: PMC10633694.
66. Bui TM, Wiesolek HL, Sumagin R. ICAM-1: A master regulator of cellular responses in inflammation, injury resolution, and tumorigenesis. J Leukoc Biol. 2020 Sep;108(3):787-799. doi: 10.1002/JLB.2MR0220-549R. Epub 2020 Mar 17. PMID: 32182390; PMCID: PMC7977775.
67. Zhang Y, Huo W, Wen Y, Li H. Silencing Nogo-B receptor inhibits penile corpus cavernosum vascular smooth muscle cell apoptosis of rats with diabetic erectile dysfunction by down-regulating ICAM-1. PLoS One. 2019 Aug 23;14(8):e0220715.
68. Wu F, Xiong ZQ, Mao SH, Hu JM, Wang JQ, Jiang HW, Ding Q. Aldosterone induces inflammatory cytokines in penile corpus cavernosum by activating the NF-κB pathway. Asian J Androl. 2018 Jan-Feb;20(1):24-29.
69. Reglero-Real N, Pérez-Gutiérrez L, Yoshimura A, Rolas L, Garrido-Mesa J, Barkaway A, Pickworth C, Saleeb RS, Gonzalez-Nuñez M, Austin-Williams SN, Cooper D, Vázquez-

Martínez L, Fu T, De Rossi G, Golding M, Voisin MB, Boulanger CM, Kubota Y, Muller WA, Tooze SA, Nightingale TD, Collinson L, Perretti M, Aksoy E, Nourshargh S. Autophagy modulates endothelial junctions to restrain neutrophil diapedesis during inflammation. Immunity. 2021 Sep 14;54(9):1989-2004.e9.

70. Simon MM, Greenaway S, White JK, Fuchs H, Gailus-Durner V, Wells S, Sorg T, Wong K, Bedu E, Cartwright EJ, Dacquin R, Djebali S, Estabel J, Graw J, Ingham NJ, Jackson IJ, Lengeling A, Mandillo S, Marvel J, Meziane H, Preitner F, Puk O, Roux M, Adams DJ, Atkins S, Ayadi A, Becker L, Blake A, Brooker D, Cater H, et al. (2013). A comparative phenotypic and genomic analysis of C57BL/6J and C57BL/6N mouse strains. Genome Biol. doi: 10.1186/gb-2013-14-7-r82.
71. Clarkson JM, Dwyer DM, Flecknell PA, Leach MC and Rowe C (2018). Handling method alters the hedonic value of reward in laboratory mice. Scientific reports. doi: 10.1038/s41598-018-20716-3.
72. Wingett SW, Andrews S. FastQ Screen: A tool for multi-genome mapping and quality control. F1000Res. 2018 Aug 24;7:1338. doi: 10.12688/f1000research.15931.2. PMID: 30254741; PMCID: PMC6124377.
73. Gustavsson EK, Zhang D, Reynolds RH, Garcia-Ruiz S, Ryten M. ggtranscript: an R package for the visualization and interpretation of transcript isoforms using ggplot2. Bioinformatics. 2022 Aug 2;38(15):3844-3846.
74. Liu S, Wang Z, Zhu R, Wang F, Cheng Y, Liu Y. Three Differential Expression Analysis Methods for RNA Sequencing: limma, EdgeR, DESeq2. J Vis Exp. 2021 Sep 18;(175).
75. Gu Z, Hübschmann D. Make Interactive Complex Heatmaps in R. Bioinformatics. 2022 Feb 7;38(5):1460-1462.
76. Lüdtke T, Steiner F, Berger T, Westermann S. Empirically Informed, Idiographic Networks of Concordant and Discordant Motives: An Experience Sampling Study With Network Analysis in Non-Clinical Participants. Clin Psychol Eur. 2025 May 28;7(2):e12305.
77. Yu G, Wang LG, Han Y, He QY. clusterProfiler: an R package for comparing biological themes among gene clusters. OMICS. 2012 May;16(5):284-7.
78. Yu G, Wang LG, Han Y, He QY. clusterProfiler: an R package for comparing biological themes among gene clusters. OMICS. 2012 May;16(5):284-7.
79. Kanehisa, M. and Goto, S.; KEGG: Kyoto Encyclopedia of Genes and Genomes. Nucleic Acids Res. 28, 27-30 (2000).
80. Kanehisa, M; Toward understanding the origin and evolution of cellular organisms. Protein Sci. 28, 1947-1951 (2019).
81. Kanehisa, M., Furumichi, M., Sato, Y., Kawashima, M. and Ishiguro-Watanabe, M.; KEGG for taxonomy-based analysis of pathways and genomes. Nucleic Acids Res. 51, D587-D592 (2023).

82. Conway JR, Lex A, Gehlenborg N. UpSetR: an R package for the visualization of intersecting sets and their properties. Bioinformatics. 2017 Sep 15;33(18):2938-2940. doi: 10.1093/bioinformatics/btx364. PMID: 28645171; PMCID: PMC5870712.

83. Zhang H, Meltzer P, Davis S. RCircos: an R package for Circos 2D track plots. BMC Bioinformatics. 2013 Aug 10;14:244.

Tables

Table 1 is available in the Supplementary Files section.

Figures

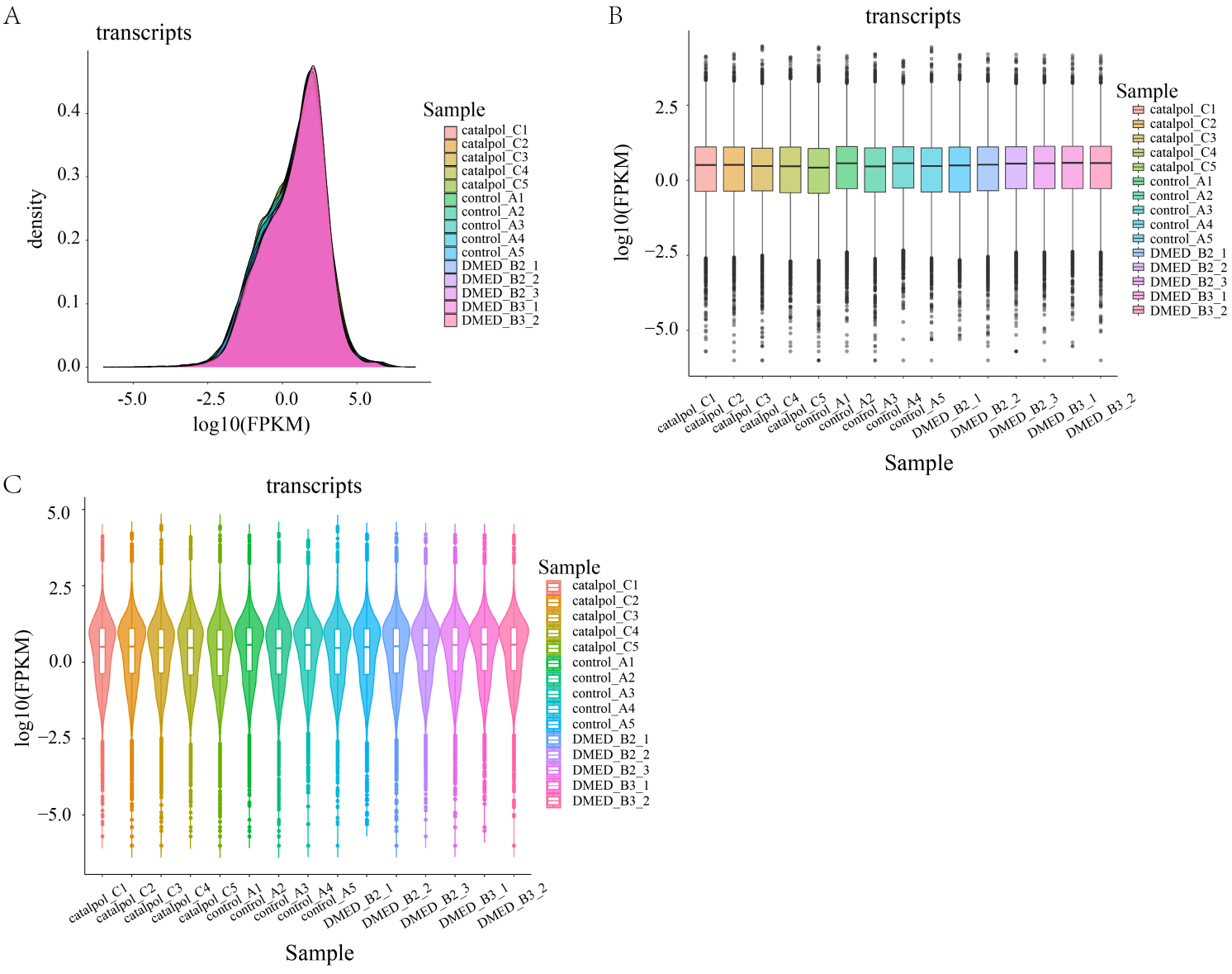


Figure 1

Quality assessment of transcriptome sequencing data. (A) Hierarchical clustering of samples based on expression levels. (B and C) Distribution of expression values across samples.

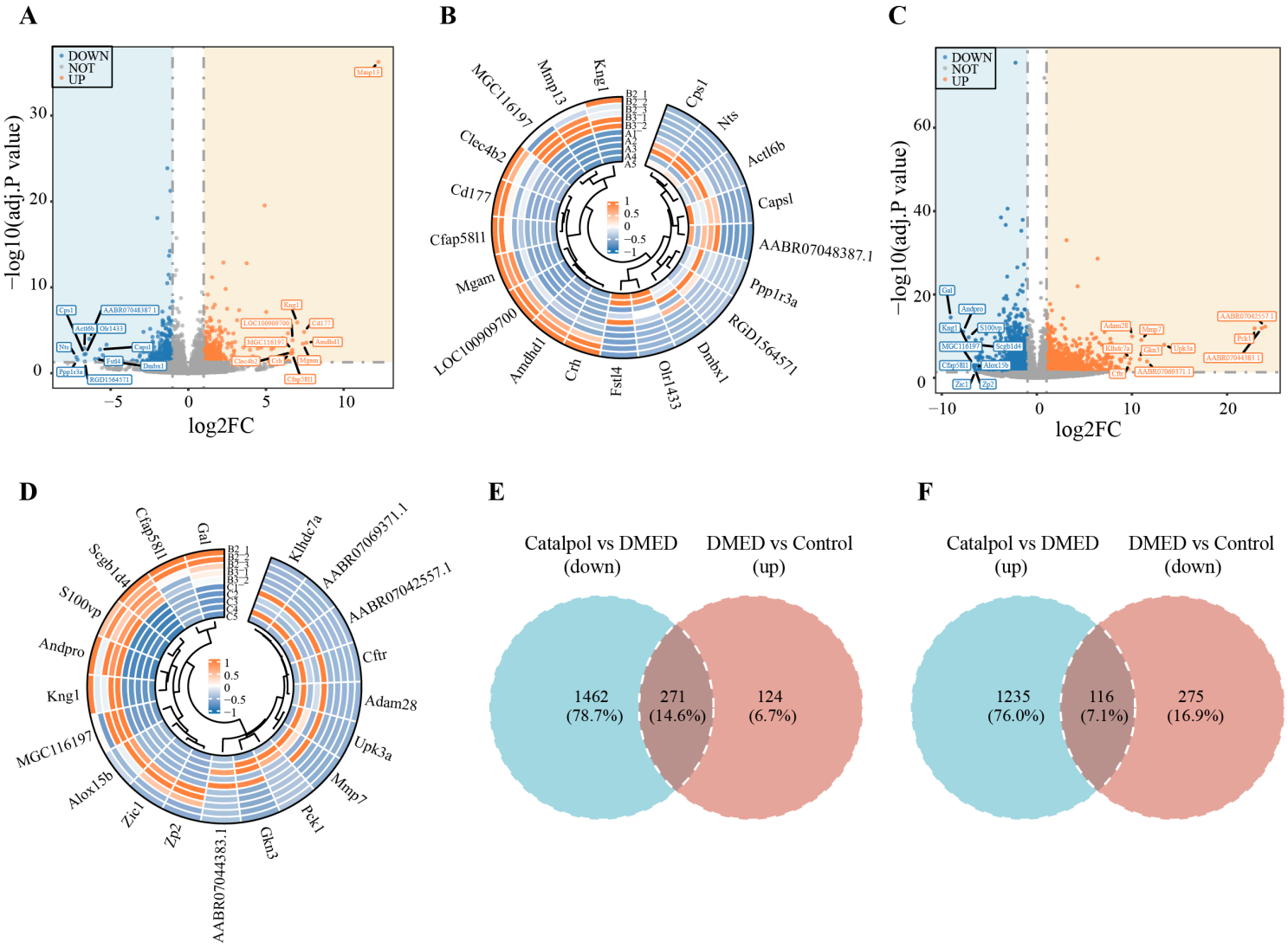


Figure 2

Differential gene expression between samples. (A and B) DEGs1 up-regulated genes and down-regulated genes differentially. (C and D) DEGs2 up-regulated genes and down-regulated gene differential expression. (E) Differential expression of DEGs1 up-regulated gene and DEGs2 down-regulated gene. (F) Differential expression of DEGs1 down-regulated gene and DEGs2 up-regulated gene.

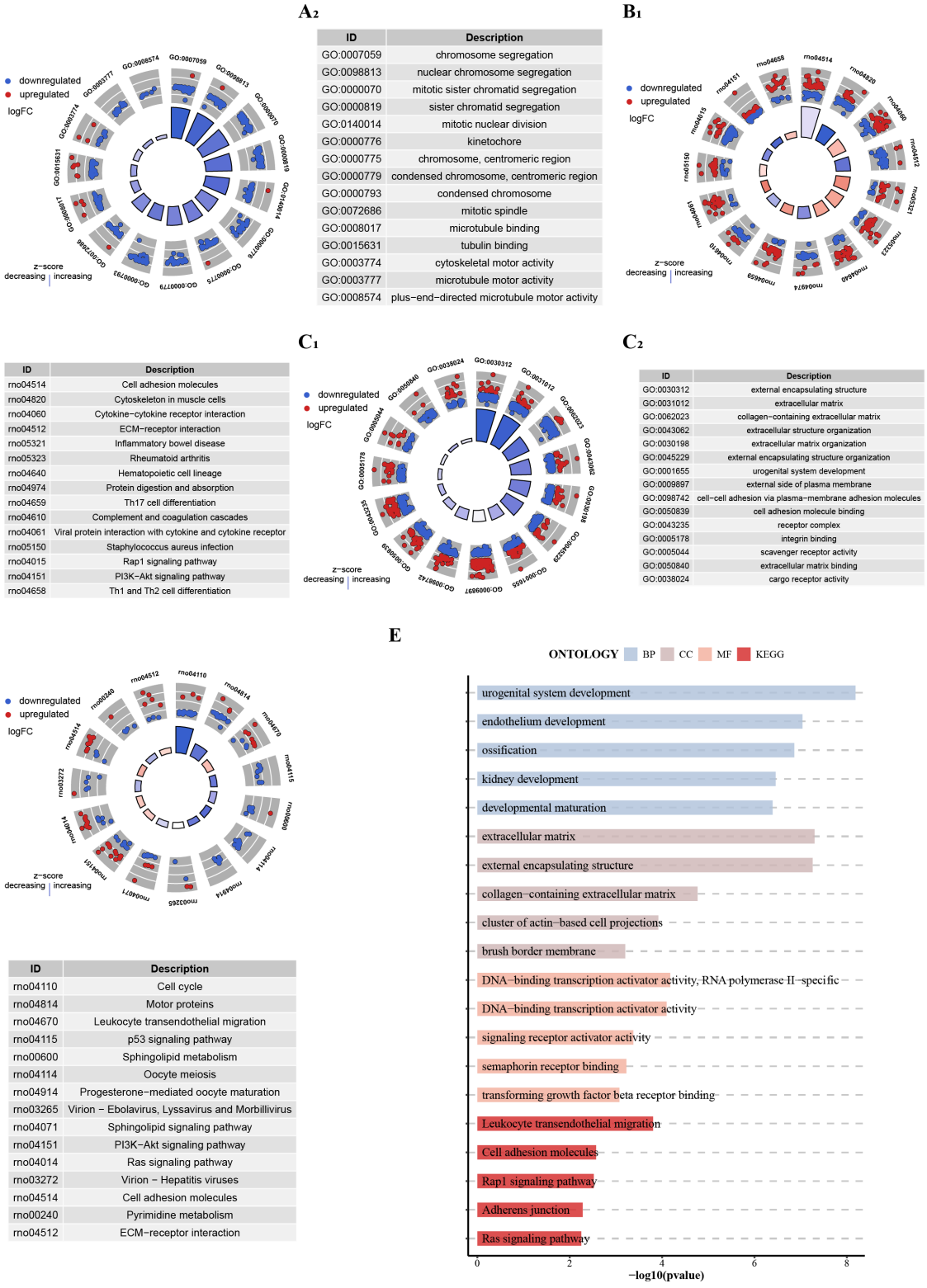


Figure 3

Enrichment analysis of biological functions related to catalpol intervention. (A_1 to B_2) DEGs1 biofunction enrichment analysis. (C_1 to D_2) DEGs2 biofunctional enrichment analysis. (E) Biological function enrichment analysis of DEGs3 catalpol intervention-related differential genes.The Kyoto Encyclopedia of Genes and Genomes (KEGG) pathway map was obtained

from KEGG(https://www.kegg.,jp/). KEGG is a publicly available resource under the terms of the academic uselicense (Kanehisa et al., 2016: Kanehisa & Goto,2000)[,31,32, 33].

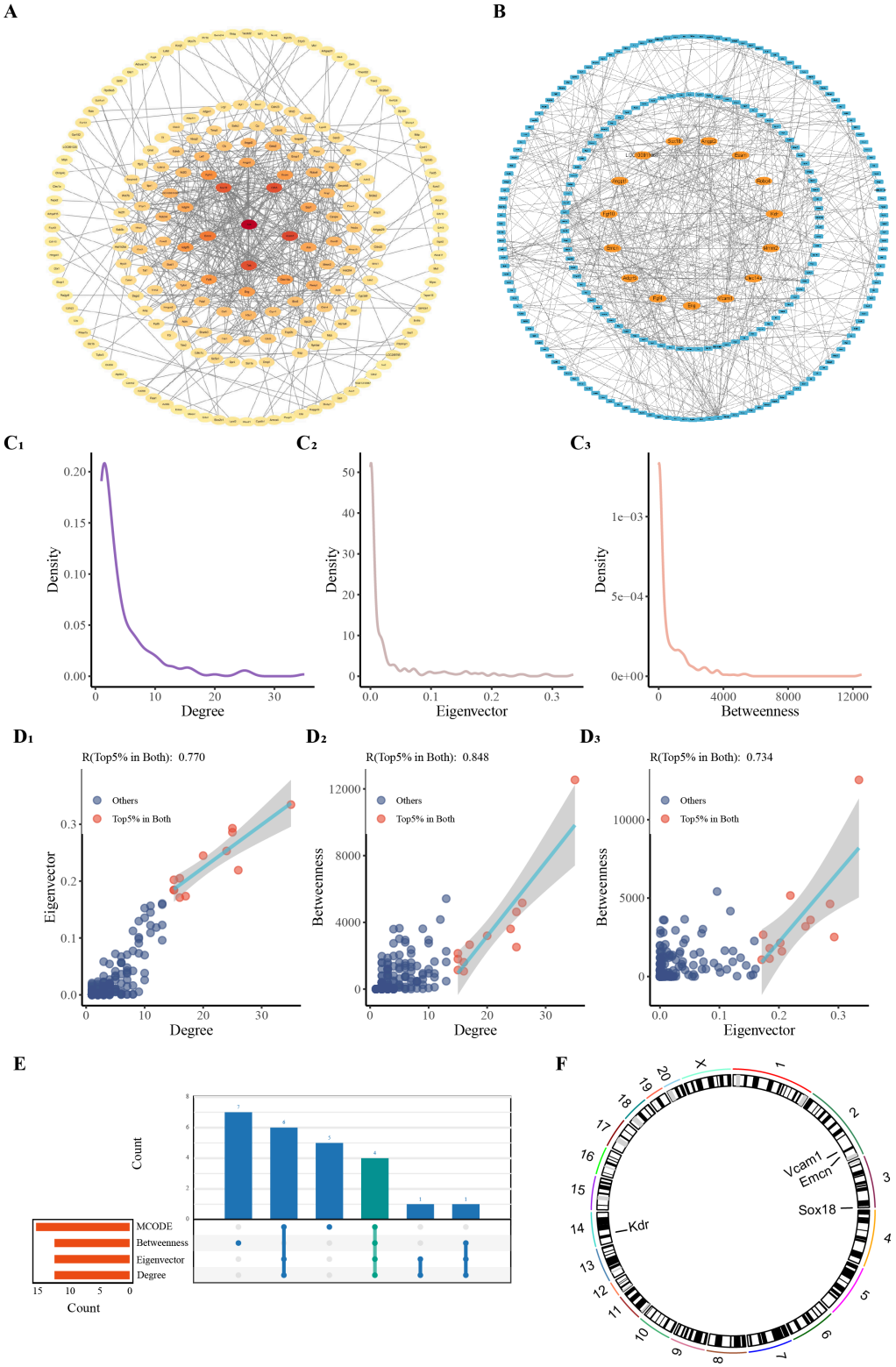


Figure 4

Analysis of differential gene centers and chromosomal localization related to catalpol intervention. (A and B) Network target genes. (C_1 to C_3) PPI network centrality analysis. (D_1

to D_3) Correlation analysis of core genes. (E) Key core gene signaling pathways. (F) Location distribution of key genes on chromosomes.

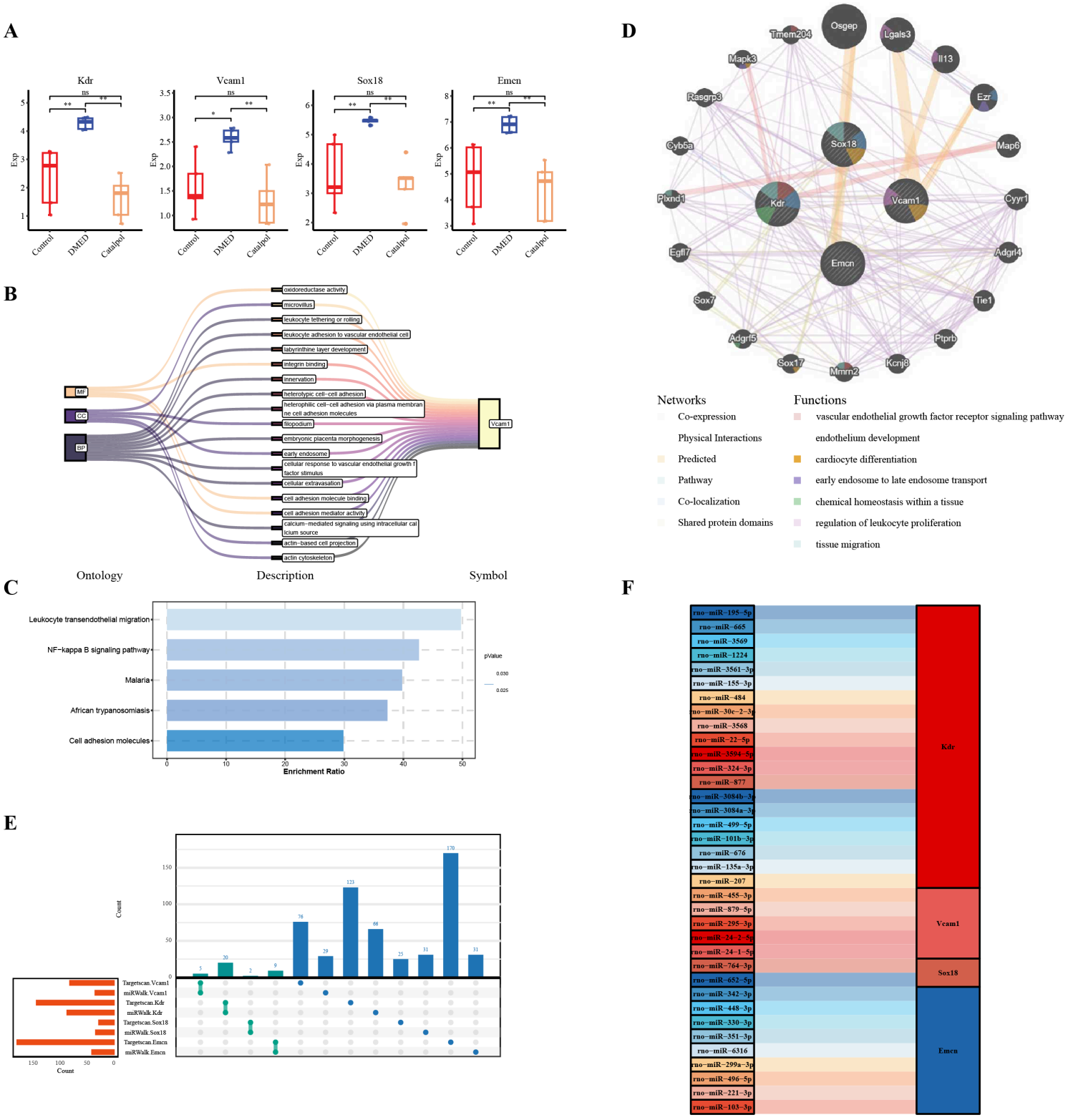


Figure 5

Core target gene expression: (A) significant difference among the three groups ($P < 0.05$), no significant difference between Control and Catalpol groups ($P > 0.05$). (B and C) Functional distribution and pathway enrichment of key genes. (D) Interactions between proteins

encoded by key genes and proteins with other related effects. (E and F) miRNA-key gene regulatory networks.

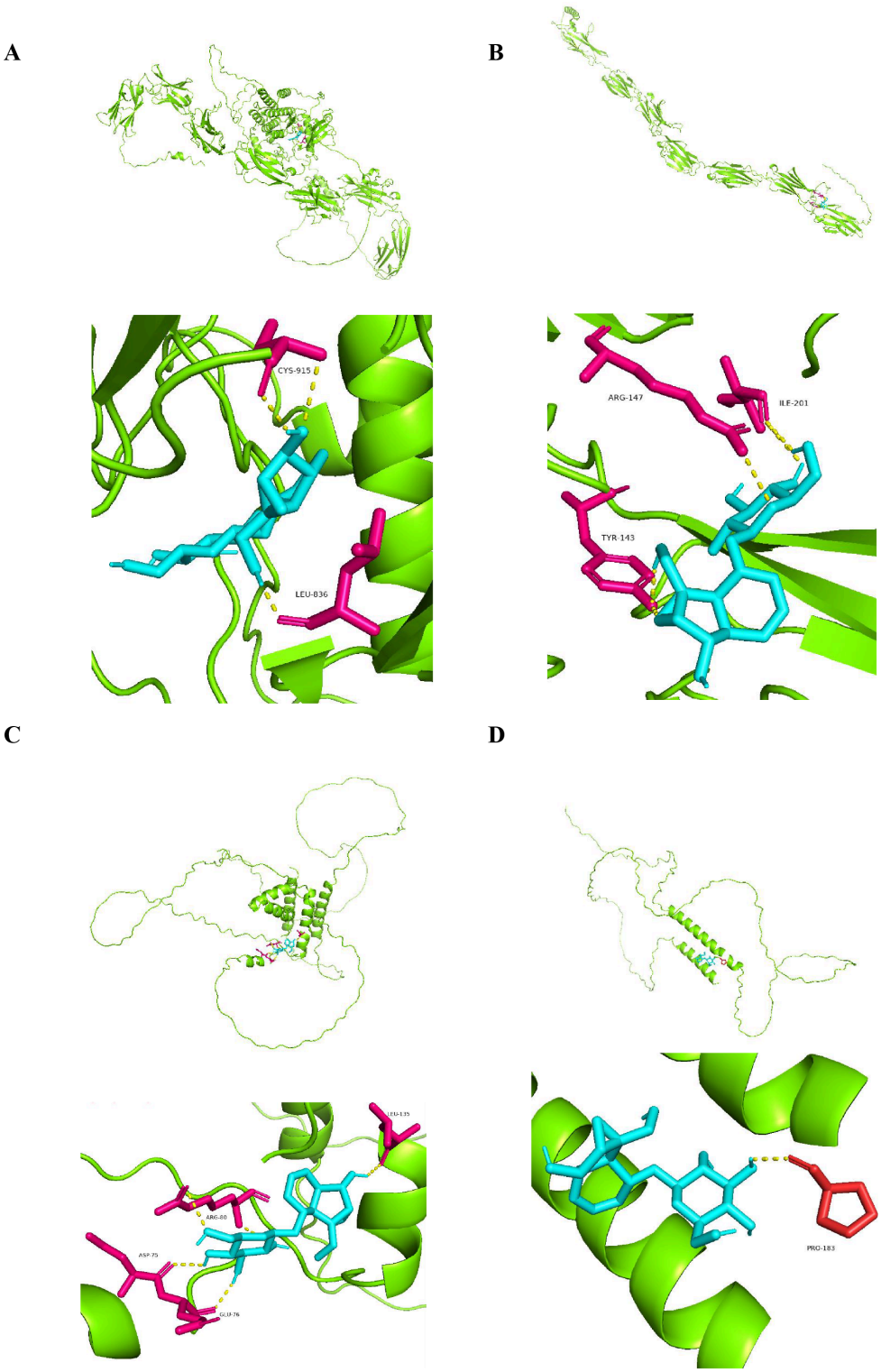


Figure 6

Molecular docking. (A) Molecular docking between Kdr and catalpol molecules. (B) Molecular docking between Vcam1 and catalpol molecules. (C) Molecular docking between Sox18 and catalpol molecules. (D) Molecular docking between Emcn and catalpol molecules.

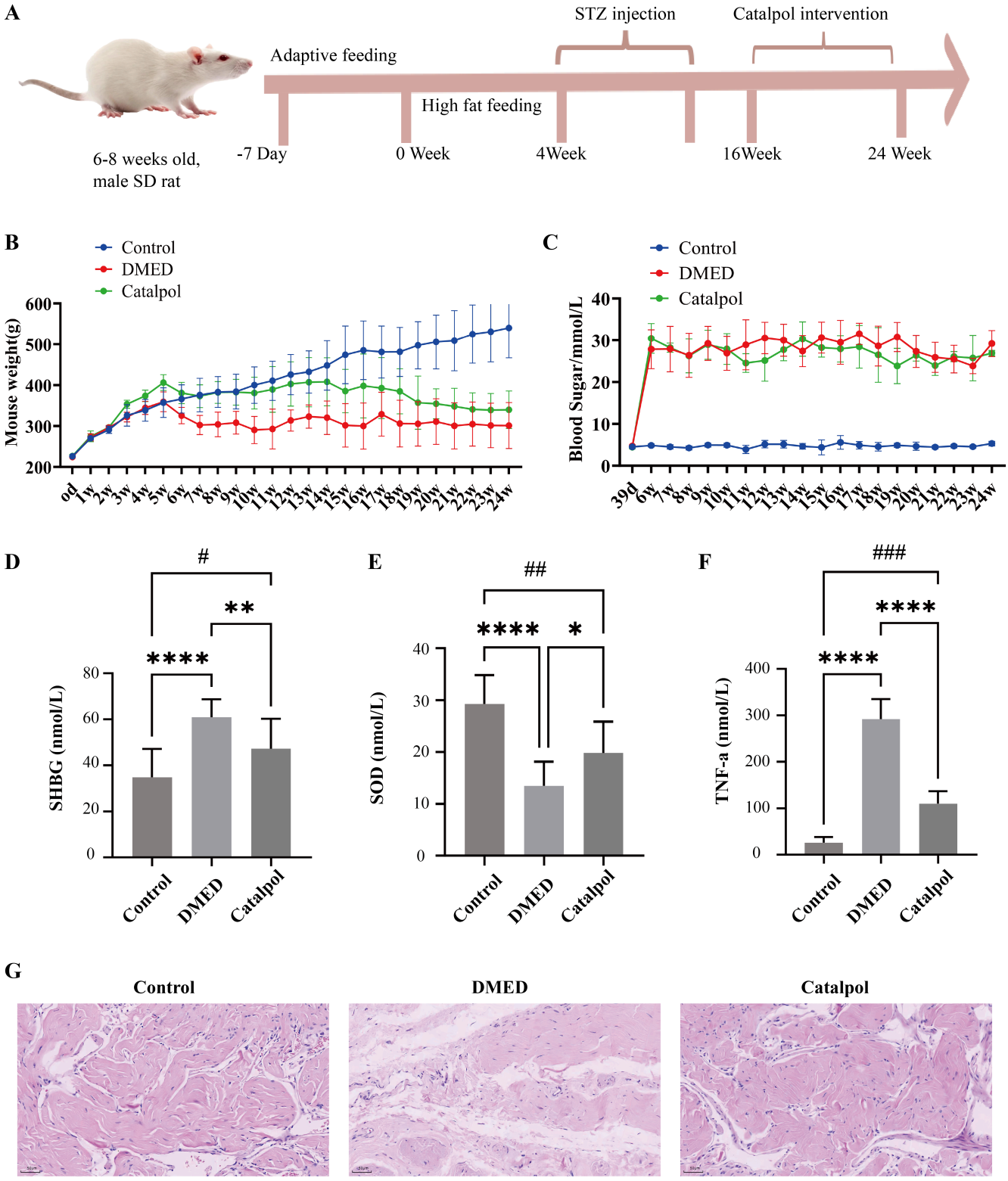


Figure 7

Modeling intervention and verification. (A) Model intervention and timeline; (B) Rat weight fluctuation levels; (C)Blood glucose fluctuation levels in rats; (D) Expression level of SHBGD; (E)Expression level of TNF-α;(F)Expression level of SOD;(G)HE staining results. In the figure, ns $P > 0.05$, *$P < 0.05$, **$P < 0.01$, ***$P < 0.001$, ****$P < 0.0001$, #$P < 0.05$, ##$P < 0.01$, ###$P < 0.001$.

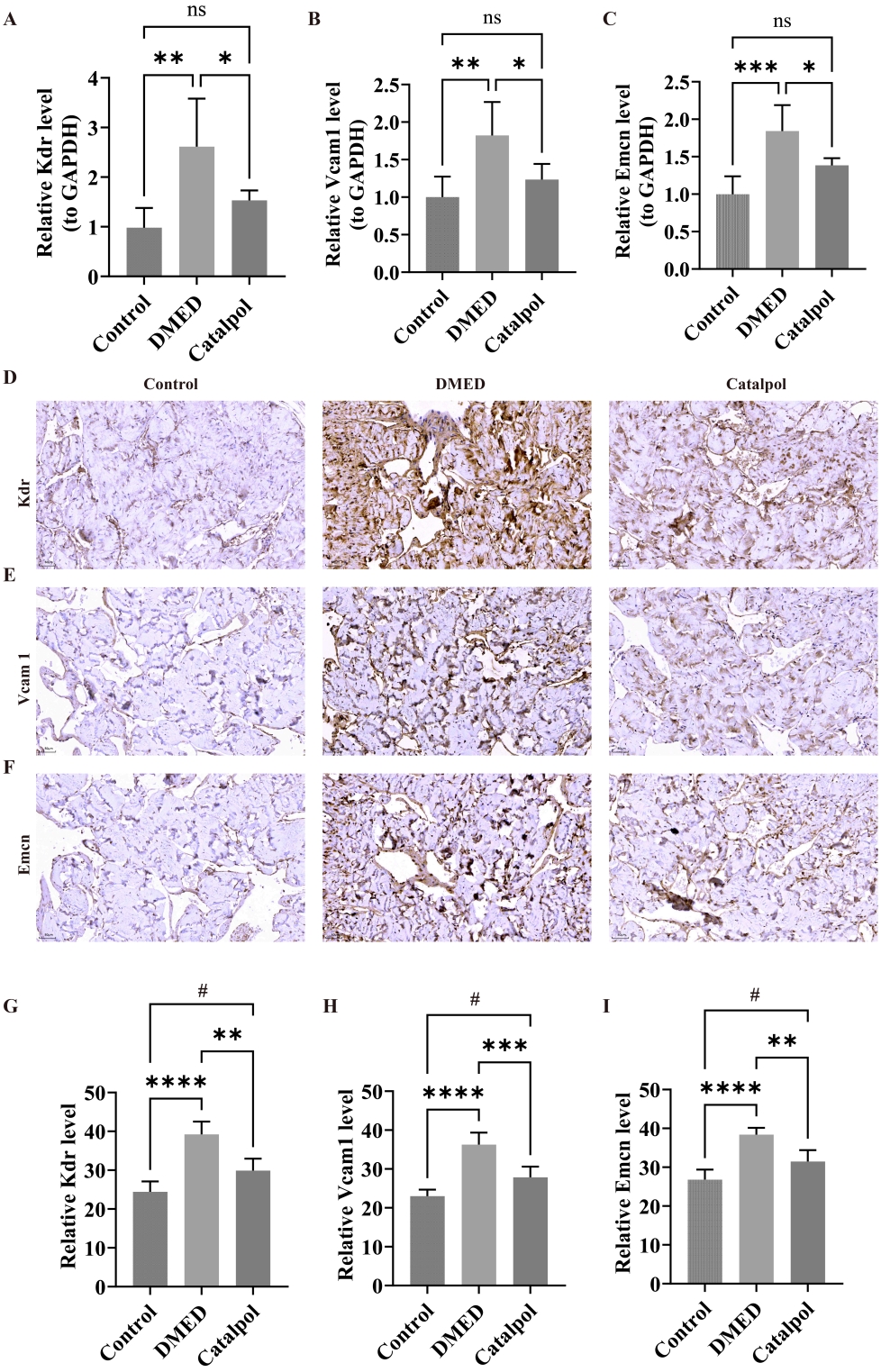


Figure 8

RT-qPCR and IHC validate core gene targets. (A to C)RT-qPCR analysis revealed that the gene expression levels of Kdr, Vcam1 and Emcn. (D to)IHC analysis revealed that the gene expression levels of Kdr, Vcam1 and Emcn.In the figure, ns $P > 0.05$, *$P < 0.05$, **$P < 0.01$, ***$P < 0.001$, ****$P < 0.0001$.$P < 0.05$.

Supplementary Files

This is a list of supplementary files associated with this preprint. Click to download.

- TableS1.TheprimersequenceofRTqPCR.xlsx
- TableS2.PrimaryantibodiesofIHC.xlsx
- TableS3.TranscriptionalDataEvaluation.xlsx
- Table1.MoleculardockingofcatalpalwithcoregenesKdrVcam1Sox18Emcn.xlsx
- TableS4.GCContentEvaluation.xlsx
- TableS5.DifferentialexpressionanalysisbetweenDMEDgroupandcontrolgroupsamples.xlsx
- TableS6.DifferentialexpressionanalysisbetweenDMEDgroupandcatalpolgroupsamples.xlsx
- TableS7.BiologicalfunctionsofDEGs1.xlsx
- TableS8.Thetop15significantlyenrichedpathwaysforDEGs1.xlsx
- TableS9.BiologicalfunctionsofDEGs2.xlsx
- TableS10.Thetop15significantlyenrichedpathwaysforDEGs2.xlsx
- TableS11.BiologicalfunctionsofDEGs3.xlsx
- TableS12.Thetop17significantlyenrichedpathwaysforDEGs3.xlsx